Desalination and Water Treatment
www.deswater.com

doi: 10.5004/dwt.2018.23299

135 (2018) 372–380
December

Adsorption of ofloxacin from aqueous solution using low-cost biochar obtained from cotton stalk

Yuan-da Du[a,†], Hong-qiang Liu[a,†], Li Shu[b], Yu Feng[a], Qiang Kong[a,*], Fei Xu[a], Qian Wang[a], Cong-cong Zhao[a]

[a]*College of Geography and Environment, Shandong Normal University, 88 Wenhua Donglu, Jinan 250014, Shandong, China, email: 392331698@qq.com (Y.-D. Du), email: 1012677821@qq.com (H.-Q. Liu), 1406490031@qq.com (Y. Feng), Tel. +86 531 86182550, Fax +86 531 86180107, email: kongqiang0531@hotmail.com (Q. Kong), xufeisdnu@yahoo.com (F. Xu), qianwang86@sdnu.edu.cn (Q. Wang), zhaocongcong1009@163.com (C.-C. Zhao)*
[b]*School of Engineering, RMIT University, 402 Swanston Street, Melbourne VIC 3000 Australia, email: li.shu846@gmail.com (L. Shu)*

Received 2 April 2018; Accepted 16 October 2018

ABSTRACT

Biochar (BC) obtained from cotton stalk was used to adsorb ofloxacin (OFL) from aqueous solution. The BC had a high surface area of 1196.24 m^2/g and adsorbed a maximum of 769.2 mg/g of OFL, and the adsorption kinetics were best represented by a pseudo-second-order kinetic model ($R^2 > 0.998$), suggesting chemisorption control. The equilibrium adsorption data were well described by the Freundlich model ($R^2 > 0.996$), indicating a multilayer adsorption process. Additionally, thermodynamic simulation indicated that the adsorption was exothermic. Finally, FTIR spectra of the BC revealed the presence of phosphorus-containing functional groups and C=O, C=C, C–O–C, P=O, P–O–C, and O–C bonds on the BC surface. Our findings indicate that BC from cotton stalk can be applied for the treatment of antibiotic-containing wastewater.

Keywords: Cotton stalk; Biochar; Ofloxacin; Adsorption

1. Introduction

Pharmaceuticals and personal care products (PPCPs) are a new pollutant commonly found in water [1]. PPCPs are widely used worldwide and are only partially absorbed; approximately 30–90% of drugs, especially antibiotics, are not directly excluded from metabolism and enter the urban sewage system. Ofloxacin (OFL) is a fluorinated quinolone antibiotic [1]. OFL can be used to cure human diseases as it is effective against gram-negative bacteria and some anaerobes [2]. In addition, a large amount of OFL has also been used as a feed additive to promote the growth of animals or administered for animal disease control [3]. However, 70–98% of OFL is excreted in human and animal feces 48 h after administration of the drug [4]. Some of the OFL can enter bodies of water through the application of fertilizer and runoff, and other parts can enter sewage treatment plants as wastewater and later enter bodies of water with the effluent from the sewage treatment plant. Currently, sewage treatment plants cannot completely remove antibiotics; therefore, a large number of antibiotics and their metabolites eventually enter water sources. The presence of OFL residues in the environment over a long period not only improves the bacteria resistance of genes but also interferes with microbial balance [5]. In addition, some resistant strains, although not pathogenic, can transfer drug-resistant genes to pathogenic bacteria, thereby increasing the risk of antibiotic residue being present in the environment and causing public health concerns. It is thus necessary to study the adsorption of OFL.

Many methods have been used for the removal or degradation of OFL, including photocatalytic degradation [6], the

*Corresponding author.

†These authors contributed equally to this work.

Presented at the 10th International Conference on Challenges in Environmental Science & Engineering (CESE-2017), 11–15 November 2017, Kunming, China

use of cork to remove OFL from aqueous solutions at different pH [7], solar irradiation [8], ozonation treatment [9], and adsorption from aqueous solutions [10]. Of these methods, adsorption is considered one of the most environmentally friendly and low-cost methods and offers many advantages compared with other conventional treatment methods; the preparation method is simple, the access to raw materials is extensive, and no nutrients are required [11].

As a new type of environmentally friendly adsorbent material, biomass material has the advantages of abundant resources, low cost, and a high adsorption rate. With the development and utilization of renewable energy, many researchers have focused on the wide range of practical uses for biological materials. Biomaterial applications are an important component of renewable energy, and the efficient exploitation and use of biomass materials will play a positive role in solving current energy and environmental issues. In China, the yield of cotton stalk is extraordinarily high (the total cotton output is 20 million tons) [12]. Although cotton stalk is widely used in various fields (e.g., the pulp and paper industry [13], animal feed [14], waste-derived catalysts [15]), it is not fully utilized because of the large output. Additionally, underutilized cotton stalks are mainly incinerated, which not only leads to a waste of biological resources but also atmospheric pollution. Therefore, it is necessary to recycle the unused cotton stalk for resource utilization. Cotton stalk provides good conditions for the preparation of biochar (BC) because of its strong regenerative ability and high cellulose, hemicellulose, and lignin contents.

In addition, cotton stalk has received increasing attention as an adsorbent for water treatment. Currently, cotton stalk adsorbent is widely used to remove dyes [12], metals [16], heavy metal ions [17], inorganic pollutants, and organic pollutants [18]. The adsorption capacity can reach a maximum of 406 mg/g, and satisfactory results have also been achieved in the removal of these pollutants. To the best of our knowledge, although there are many application materials for antibiotic removal (e.g., *Albizia lebbeck* seed pods [19], luffa sponge [11], reed straw [20]), antibiotic adsorption by adsorbent produced from cotton stalk has not yet been reported. Therefore, we were motivated to take advantage of cotton stalk agricultural waste to treat antibiotic-containing wastewater.

The objective of this study was to investigate the efficiency of BC obtained from cotton stalk in adsorbing OFL from aqueous solution and to provide a basis for the application of cotton stalk adsorbent in treating antibiotic-containing wastewater. The BC was characterized using scanning electron microscopy (SEM), Brunauer–Emmett–Teller (BET) analysis, X-ray diffraction (XRD), and Fourier-transform infrared (FTIR) spectroscopy. Additionally, the adsorption mechanism was investigated by applying adsorption kinetic models, adsorption isotherm models, and thermodynamic models.

2. Methods and materials

2.1. Materials

Cotton stalk was collected from Jinan, Shandong Province, China. First, the cotton stalk was washed with distilled water. After drying in an oven at 70°C (24 h), the cotton stalk was broken into lengths of 3–4 mm. The dried cotton stalk was then treated with phosphoric acid at a solid:liquid ratio of 1:3.5 (v/v) (30 h, 25°C). To prepare the BC, the cotton stalk was then carbonized in a muffle furnace (2 h, 400°C). The cotton stalk BC samples were then washed until a neutral pH was reached and then dried in an oven (48 h, 70°C). Finally, the carbonized cotton stalk samples were ground into a 200-mesh powder.

2.2. BC characterization

SEM (SUPRATM55, Zeiss Company, Germany) was used to investigate the specific surface structural and surface morphology characteristics of the BC. Surface area analysis of the BC was performed using N_2 adsorption–desorption isotherms (Quantachrome, USA). BET analysis was used to visualize the porous properties (Quantachrome, USA). XRD was performed to examine the sample structures using a voltage of 40 kV, current of 40 mA, and DS1° slit in the range of 5°–80°. The surface chemical functional groups and elemental composition of the BC samples were also determined using FTIR spectroscopy (Thermo Scientific, USA).

2.3. Adsorption experiments

The OFL (C18H20FN3O4, MW = 361.37 g/mol) used in this study was obtained from Sangon Company (Shanghai, China). All the batch adsorption experiments were performed in a temperature-controlled oscillator (25°C, 180 rpm). The OFL solutions at different concentrations were obtained by diluting the stock solution. The OFL solution absorbances were determined using an ultraviolet spectrophotometer at 294 nm. The OFL concentration was calculated from the OFL standard curve. In this study, each batch of experiments had three replicates and one blank. The OFL adsorbed by the adsorbent Q_e (mg/g) is expressed as

$$Q_e = \frac{(C_0 - C_e)V}{w} \tag{1}$$

where C_0 and C_e (mg/L) are the OFL concentrations initially and at equilibrium, respectively; V (L) is the solution volume; and W (g) is the mass of BC. The percentage removal R_e (%) of OFL is expressed as

$$R_e = \frac{C_0 - C_e}{C_0} \times 100 \tag{2}$$

2.4. BC isoelectric point test

The charge of the ampholyte varies with the pH value of the solution. When the values of positive and negative charges of the two electrolytes are equal, the pH value of the solution is called the isoelectric point of the substance. The isoelectric point of BC was used to determine the zeta potential at different pH = 1–12 at the same BC concentration using a zeta potentiometer. The zeta potential was determined by measuring the electrophoresis rate by measuring the Doppler displacement of the scattered laser. The isoelectric point of the BC was considered the point at which the electric potential was zero.

2.5. Adsorption kinetics

The adsorption kinetics were investigated to determine the kinetic parameters and examine the adsorption mechanism. OFL adsorption onto the BC was examined using batch experiments. First, 40 mg of BC was introduced into 50 mL of OFL solutions with initial concentrations of 50, 100, and 200 mg/L for 10, 30, 60, 90, 120, 150, 180, 240, 300, and 360 min. The adsorption mechanism was investigated by fitting pseudo-first and pseudo-second order kinetic models and an intraparticle diffusion equation to the experimental data.

The pseudo-first-order kinetic model [21] is expressed as

$$\ln\left(Q_e - Q_t\right) = \ln Q_e K_1 t \tag{3}$$

where Q_e (mg/g) and Q_t (mg/g) are the amounts of OFL adsorbed at equilibrium and at time t (min), respectively, and k_1 (1/min) is the rate constant.

The pseudo-second-order equation [22] is expressed as

$$\frac{t}{Q_t} = \frac{1}{K_2 Q_e^{\,2}} + \frac{t}{Q_e} = \frac{1}{V_0} + \frac{t}{Q_e} \tag{4}$$

where k_2 (g/(mg min)) is the rate constant; Q_e (mg/g) and Q_t (mg/g) are the amount of OFL adsorbed at equilibrium and at time t (min), respectively; and V_0 (mg·g^{-1} min^{-1}) is the initial sorption rate.

The intraparticle diffusion equation [23] is expressed as

$$Q_t = K_p t^{1/2} + C \tag{5}$$

where k_p [mg/(g min$^{1/2}$)] is the rate constant.

2.6. Adsorption isotherms

The performance of BC was evaluated by performing adsorption isotherm experiments. The isotherm of OFL adsorption on BC was obtained by performing adsorption tests. BC (40 mg) was added to 100-mL conical flasks containing 50 mL of OFL solutions at seven different initial concentrations (30–180 mg/L) at 298 K, 303 K, and 313 K.

Three well-known isotherm equations, namely the Langmuir, Freundlich, and Dubinin–Radushkevich models, were applied to determine the adsorption mechanism.

The Langmuir model [24] is generally expressed as

$$\frac{C_e}{Q_e} = \frac{1}{Q_m K_L} + \frac{C_e}{Q_m} \tag{6}$$

where Q_e (mg/g) is the amount of OFL adsorbed and C_e (mg/L) is the OFL concentration at equilibrium, Q_m (mg/g) is the maximum OFL adsorption capacity, and k_L (L/mg) is the Langmuir constant.

The Freundlich model [25] is generally expressed as

$$\ln Q_e = \ln K_F + \frac{1}{n} C_e \tag{7}$$

where K_F is the relative adsorption capacity of BC and 1/n is a constant associated with the adsorption intensity or surface heterogeneity.

The Dubinin–Radushkevich model [26] is expressed as

$$\ln Q_e = \ln Q_m - \beta\varepsilon^2 \tag{8}$$

$$\varepsilon = RT \ln\left(1 + 1/C_e\right) \tag{9}$$

$$E = 1/(2\beta)^{1/2} \tag{10}$$

where Q_e (mg/g) is the amount of OFL adsorbed and Q_m (mg/g) is the maximum adsorption capacity of BC at adsorption equilibrium; E (kJ/mol) is the average adsorption free energy; T (K) is the thermodynamic temperature; R is the ideal gas constant [8.314 J/(mol K)]; and β (kJ^2/mol^2) and ε are constants corresponding to the adsorption energy and Polanyi potential, respectively.

2.7. Adsorption thermodynamics

The thermodynamic [27] behavior of OFL adsorption onto BC was evaluated by investigating the thermodynamic parameters, including the change in the free energy (ΔG), enthalpy (ΔH), and entropy (ΔS):

$$\ln K_L = \Delta S/R - \Delta H/RT \tag{11}$$

$$\Delta G = -RT \ln K_L \tag{12}$$

where R is the ideal gas constant [8.314 J/(mol K)], K_L (L/mol) is the Langmuir isotherm constant, T (K) is the thermodynamic temperature of the solution, ΔG is the standard Gibbs free energy change, ΔH is the enthalpy change, and ΔS is the entropy change.

3. Results and discussion

3.1. BC characterization

SEM is an effective analysis technique for evaluation of a sample surface. When the surface of the BC was magnified 5000 times, some particles and pores were clearly observed, which reflected the change in BC prepared from cotton stalk before and after OFL adsorption (Fig. 1). The surface structure of BC before adsorption was coarse with a heterogeneous surface and abundant pores. Additionally, Fig. 1a reveals a large number of smaller pores in the inner walls of the pores, indicating that the porous nature of BC is advantageous for the adsorption of OFL molecules. In contrast, after adsorption, many pores were filled with OFL molecules (Fig. 1b), indicating that these pores of the BC surface are involved in the adsorption process of OFL and have a high adsorption capacity.

The BC had a well-developed porous structure, as shown in Fig. 2a. The pore size of the BC was mainly distributed between 1 and 20 nm and mainly concentrated in the mesoporous range. In addition, the pore size was relatively concentrated at 1–7 nm, and the pore volume reached a maximum when the pore size was less than 2 nm, indicating that the BC prepared from cotton stalk has a mesoporous mixed structure. The pore size distribution in the BC indicates that 80% of the pores were mesopores (diameters of 2–50 nm), with micropores (diameters < 2

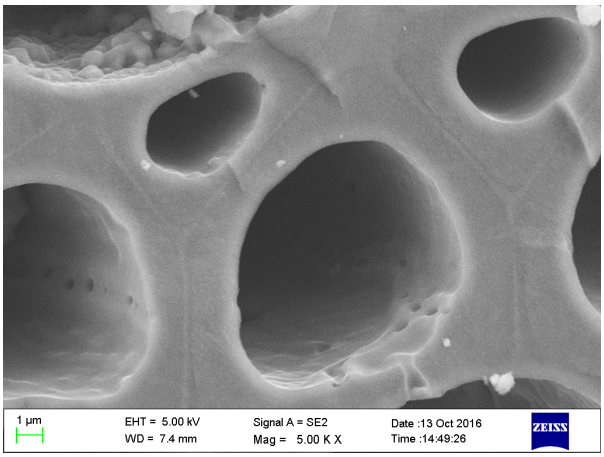

(a)

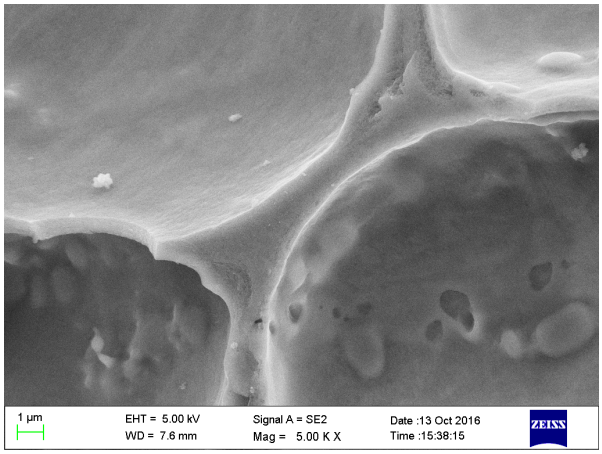

(b)

Fig. 1. SEM images of BC before (a) and after (b) OFL adsorption.

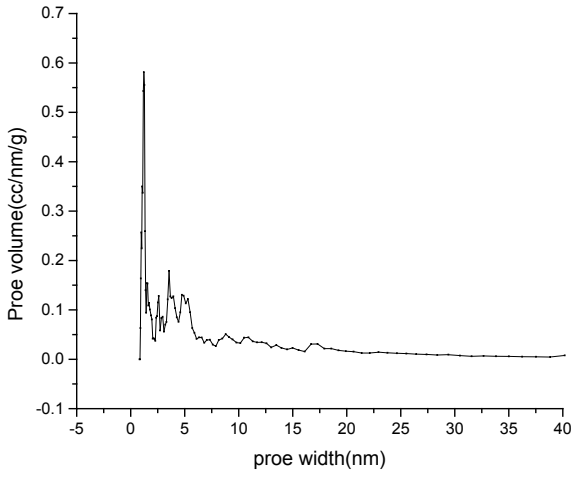

(a)

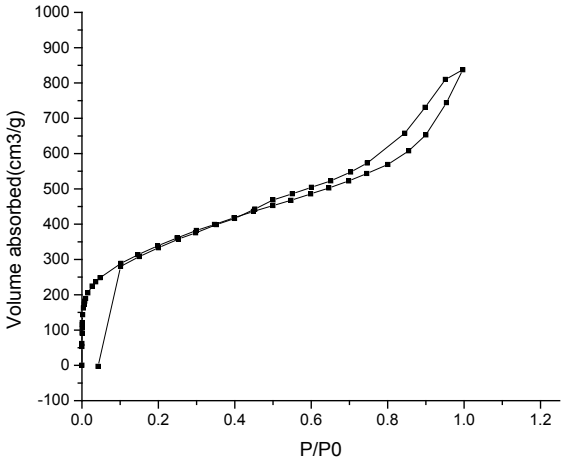

(b)

Fig. 2. Pore size distribution (a) and N_2 adsorption/desorption isotherms (b) of BC.

nm) accounting for 20% and no macropores (diameters > 50 nm) [28]. The N_2 adsorption/desorption isotherms were characterized as a mixture of types I and IV, as shown in Fig. 2b; in the low-pressure range, the amount of gas adsorbed rapidly increased with increasing pressure until reaching a limit [29]. Hysteresis loops appeared in the high-voltage range, and capillary condensation was observed in the adsorption. These findings indicate that the BC was a microporous and mesoporous composite structure [30]. The adsorption of bio-carbon on macromolecules thus has great advantages; therefore, the BC can effectively adsorb OFL molecules. Additionally, the BET surface area of BC was 1196.224 m^2/g, which is clearly higher than those of loofah sponge BC (842.3 m^2/g) [31], rice husk BC(480 m^2/g) [32], and wood BC (273 m^2/g) [33]. Therefore, BC prepared from cotton stalk is potentially a good OFL adsorbent.

3.2. FTIR analysis

FTIR spectroscopy can be used to determine the change in functional groups of BC before and after adsorption, and the function of the functional groups in the adsorption process is shown in Fig. 3. The positions of BC before and after the adsorption of OFL were almost coincident; however, the vibration frequency of the peak after the adsorption was weakened, indicating that these functional groups were occulted by OFL molecules during the adsorption process. However, a new peak appeared at 3,700 cm^{-1} after adsorption, representing the stretching of O–H or dehydration of holocellulose [34]. In addition, in the range of 1300–900 cm^{-1}, absorption peaks are often produced by phosphorus-containing functional groups, such P=O and P–O–C, which indicated that after activation, functional groups appeared on the BC surface [35]. The peak at 1230 cm^{-1} is attributed to the telescopic vibration of C–O. The peak at 1600 cm^{-1} is attributed to benzene rings or C=C bond stretching vibrations, and the absorption peaks in the 1500–1750 cm^{-1} range are attributed to C=O bond vibrations, indicating that the raw material has an aromatic structure. The broad absorption band in the range of 2500–3900 cm^{-1} is a characteristic of the vibration of hydroxyl or dehydration of the holocellulose [36]. These results indicate that abundant phos-

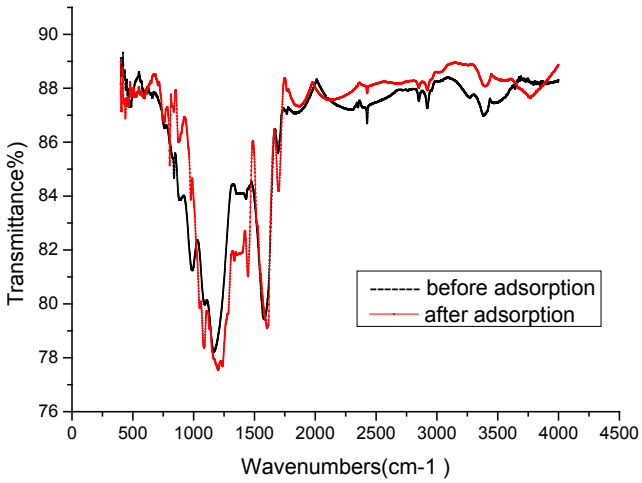

Fig. 3. FTIR spectra of BC before and after OFL adsorption.

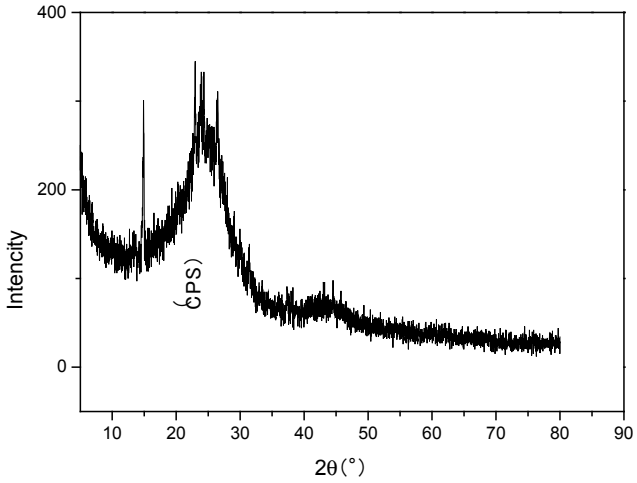

Fig. 4. XRD profiles of BC.

phorus-containing groups and C–O, C=O, C=C, P=O, and P–O–C were detected on the BC surface.

3.3. XRD study

An XRD pattern of the BC prepared from cotton stalk is presented in Fig. 4. The peak at 15° (2θ) indicates that the BC contains a completely ordered region of cellulose, i.e., the crystal plane is retained in the XRD spectrum and the cellulose is still partly crystalline [37]. In addition, the peak at approximately 23° (2θ) corresponds to the dispersion of graphite bands, which indicates that the BC has a high ash content and is carbon-rich. During the carbonization process, the structure of BC gradually forms graphite-like crystalline microcrystals superimposed by several layers with more irregular aromatic pores [38]. The results indicate that the high graphitization degree of bio-carbon and the irregular aromatic pores are beneficial to the adsorption of OFL by bio-carbon. In addition, the graphitization degree of BC was high, and the irregular aromatic pores were favorable for the adsorption of OFL by BC.

3.2. Adsorption experiment

3.2.1. Effect of adsorbent dosage

The OFL removal rate initially increased from 37% to 98% with increasing BC dosage from 0.2 to 1.2 g/L (Fig. 5). The gradual increase occurred because the number of available adsorption sites of BC for OFL adsorption increased with increasing adsorbent dosage. Thus, OFL molecules had more chances to adhere to the adsorption sites. Despite the increase in the removal rate, the OFL equilibrium adsorption amount decreased from 206 to 90 mg/g because fewer OFL molecules could be adsorbed by the adsorption sites and competition for adsorption of OFL was obvious with increasing excessive BC dosage [34]. When the amount of BC was 0.8 g/L, the removal efficiency of BC was close to 100%. Therefore, 0.8 g/L was selected as the amount of BC added in the subsequent tests.

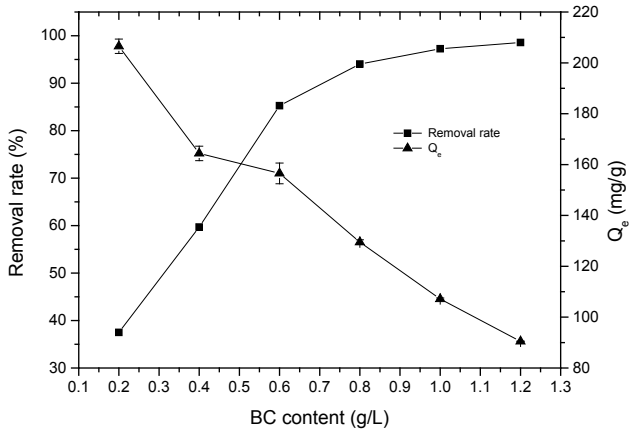

Fig. 5. Effect of BC dosage on removal rate and adsorption capacity.

3.2.2. Effect of OFL initial concentration

The OFL removal rate decreased from 99% to 86.4% with increasing initial OFL concentration from 20 to 120 mg/L, whereas the adsorption capacity increased from 29 to 145 mg/g (Fig. 6). The removal rate decreased because the BC dosage was kept constant; therefore, the number of vacant active sites was limited and saturated at low OFL concentrations. Correspondingly, as the initial concentration increased, the driving force for mass transfer increased, thereby promoting the motion of OFL molecules in the solution on the particle surface and resulting in an increase of the adsorption rate [38]. However, the equilibrium adsorption capacity increased because the higher initial concentration of OFL intensified the adsorption capacity initially [31,39]. The concentrations of antibiotics detected in domestic effluents and pharmaceutical manufacturing facility effluents can reach levels of nanograms per liter [40] and milligrams per liter [41], respectively. To better embody the adsorption effect of bio-carbon, the concentration of OFL in subsequent experiments was set at 100 mg/L.

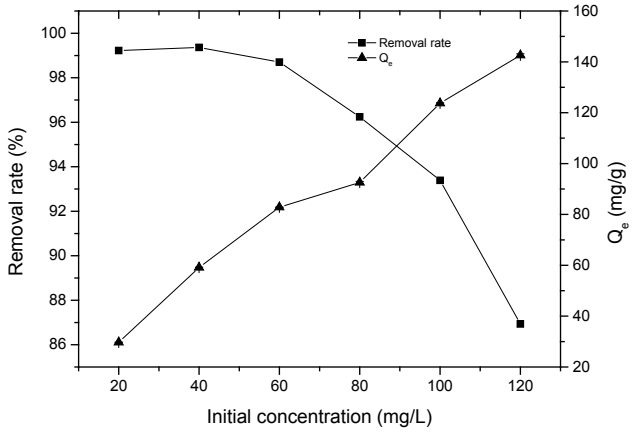

Fig. 6. Effect of initial OFL concentration on removal rate and adsorption capacity.

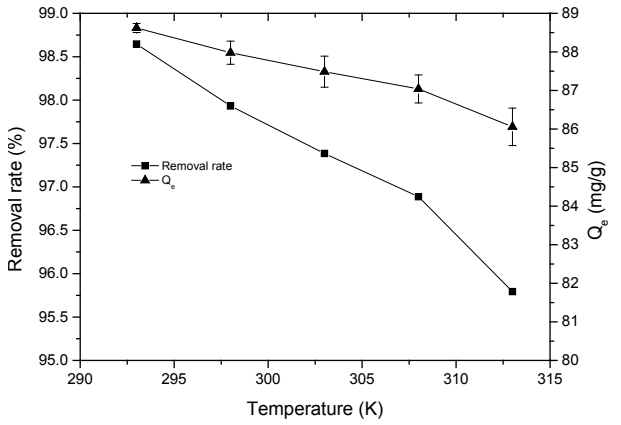

Fig. 7. Effect of temperature on removal rate and adsorption capacity.

3.2.3. Effect of temperature

The removal rate decreased slightly from 98.7% to 95.3% and the adsorption capacity decreased from 88.44 to 86 mg/g upon increasing the temperature from 293K to 313K (Fig. 7), indicating that the adsorption process of OFL by BC was exothermic adsorption. This finding suggests that the removal rate of OFL decreased with increasing temperature owing to the adsorptive major forces involved in molecule binding, which might be weakened with increasing temperature [42]. Similar adsorption behaviors have been previously reported for other adsorbents [43,44].

3.2.4. Effect of time

Increasing the contact time resulted in rapid increases of the removal rate from 68% to 92% and of the equilibrium adsorption capacity from 86 to 117 mg/g within the first 120 min (Fig. 8). These rapid increases are attributed to the large number of unsaturated surface and adsorption sites available on the BC surface area and the OFL molecules being easily adsorbed by these sites. Nevertheless, from 120 to 240 min, the removal rate increased slowly from 92% to 97% and the equilibrium adsorption capacity increased slowly from 117 to 124 mg/g. These slower increases were caused by more OFL molecules being adhered to the surface of BC during the adsorption process. The number of available adsorption sites therefore decreased [38]. After 240 min, the adsorption rate and adsorption capacity remained almost constant, indicating that adsorption equilibrium was reached. Equilibrium was achieved because the surface adsorption sites of BC reached saturation at 240 min [45]. The results indicate that the optimal contact time should be a minimum of 240 min.

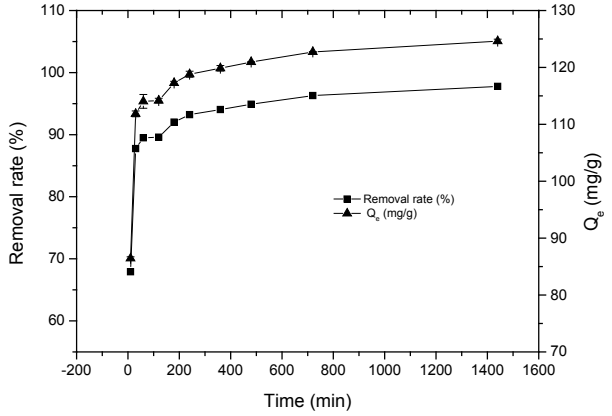

Fig. 8. Effect of time on adsorption efficiency.

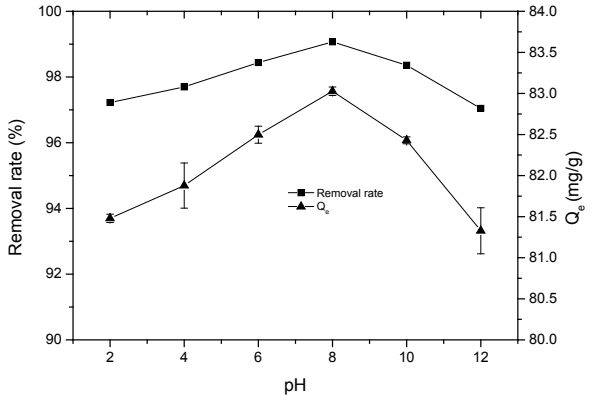

Fig. 9. Effect of solution pH on removal rate and adsorption quantity.

3.2.5. Effect of pH

The effect of pH on the removal rate and adsorption amount of OFL from BC is shown in Fig. 9. The removal rate and adsorption amount of BC on OFL gradually increased to 99% and 82.7 mg/g, respectively, before gradually decreasing upon continuing to increase the pH. Fig. 7 shows that the maximum removal rate and maximum adsorption amount of OFL were achieved at pH = 8. The optimal pH is also consistent with one of the dissociation constants of OFL (pK_1 = 5.77, pK_2 = 8.44), and similar adsorption behaviors have previously been reported [19]. When the solution pH is less than 5.77, OFL exists in the form of a cation; when

the solution pH is less than 8.44, OFL exists in the form of mixed anions and cations; and when the solution pH is greater than 8.44, OFL mainly exists in the form of anions. Therefore, OFL can have many different forms in aqueous solutions. The charge of the amphoteric ions varies with the pH of the solution, and when the numbers of positive and negative ions are equal, the pH value of the solution is the isoelectric point. The isoelectric point of the BC is shown in Fig. 10. The isoelectric point (pI) of BC prepared from cotton straw is approximately 2.3. The charges of the amphoteric ions varied with the pH of the solution. When the values of the positive and negative ions of the amphoteric ions were equal, the pH of the solution was at its isoelectric point. When the pH of the external solution was greater than the pI = 2.3 value of the amphoteric ions, the amphoteric ions released a negative charge. When the pH of the external solution was less than the pI = 2.3 value of the amphoteric ion, the amphoteric ion was positively charged. When the pH of the solution was in the range of 2.3 < pH < 8.44, the BC particles dispersed in the solution were negatively charged. The OFL was in the form of cationic and mixed ions, and the surface negative charge of BC could attract electrolyte ions with opposite charges. Therefore, when the solution pH was less than 8, the removal rate and adsorption amount of bio-carbon on OFL gradually increased. In addition, when the pH was greater than 8, OFL was present in the form of anions; therefore, the removal rate and adsorption amount gradually decreased. When the pH value of the solution was less than 8, the removal rate and adsorption amount of BC on OFL gradually increased. In addition, when the pH value was greater than 8, OFL existed in the form of anions; therefore, the removal rate and adsorption amount gradually decreased. The value of initial pH was thus adjusted to 8 for subsequent experiments.

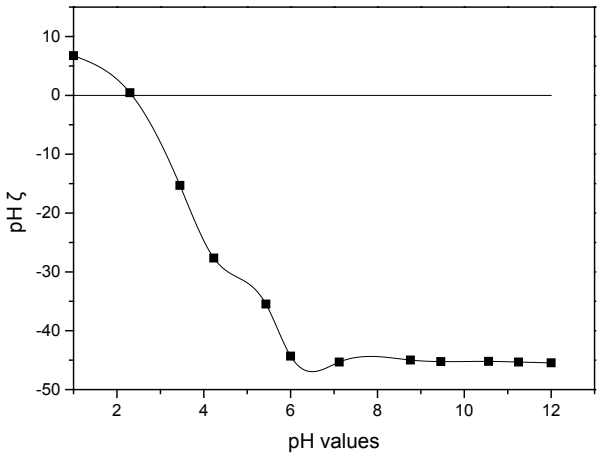

Fig. 10. Zeta potential under different pH.

3.3. Kinetic models

The adsorption data of BC adsorption of OFL were processed using kinetic models, and the results are summarized in Table 1. The comparisons with the pseudo-first-order kinetics and particle internal diffusion model curves were not consistent with the experimental data. However, the higher R^2 ($R^2 > 0.99$) and low Δq (%) values indicate that the pseudo-second-order kinetic model shows a fairly high degree of consistency. Therefore, the BC adsorption process of OFL can be described by a quasi-second-order kinetic model, and the Q_e of this model is most consistent with the experimental data (Q_{exp}). This finding indicates that the rate of adsorption is controlled by chemical adsorption of valence force through the exchange or sharing of electrons [46]. The pseudo-second-order kinetic model indicates that chemistry controls the adsorption removal rate and that the adsorption capacity is proportional to the number of active sites on the adsorbent.

3.4. Adsorption isotherm studies

The adsorption isotherm studies provided critical information on the distribution of the OFL molecules between the aqueous solution and solid. The fitting of data with three different models described in section 2.6 was an important step for optimizing the performance of adsorbents as well as the adsorption capacity. The adsorption equilibrium isotherms of OFL on BC are summarized in Table 2. The Langmuir model and Dubinin–Radushkevich model could not explain the adsorption process of BC well because of the low R^2 fitting. However, the R^2 fitting degree of the Freundlich model was significantly higher than those of the other two models. Therefore, biosorption of OFL onto BC can be described by the Freundlich model, which suggests that the adsorption process can be modeled by a multi-layer adsorption mechanism. Furthermore, this finding indicates that the adsorption occurs on heterogeneous surfaces. The main adsorption forces between BC particles and OFL molecules and the functional groups on the surface of BC lead to its heterogeneity, which is also consistent with the kinetic model for the chemical adsorption by BC [47]. The values of 1/n were between 0 and 1, which indicates that the adsorption process of OFL is favorable. The maximum adsorption capacity decreased from 769 to 555 mg/g upon increasing

Table 1
Parameters for three kinetic models of OFL adsorption

Pseudo-first-order kinetics						Pseudo-second-order kinetics					Particle diffusion model		
Concentration (mg/l)	Exp-data Q_e (mg/g)	k_1 (min^{-1})	Q_e (mg/g)	R^2	Δq (%)	k_2 (g mg^{-1} g^{-1})	Q_e (mg/g)	R^2	Δq (%)	K_p (mg g^{-1} $min^{-1/2}$)	C (mg/g)	R^2	Δq (%)
50	74.28	0.0025	13.46	0.950	2.10	0.1333	68.02	0.999	1.66	0.99	43.47	0.877	3.23
100	134.23	0.0126	81.00	0.963	3.83	0.0293	149.00	0.999	1.34	1.69	98.34	0.784	2.67
200	191.20	0.0199	232.16	0.948	1.95	0.0434	208.33	0.998	1.55	2.78	153.75	0.899	4.82

Table 2
Correlation parameters for Langmuir, Freundlich, and Dubinin–Radushkevich adsorption isotherms

Langmuir model				Freundlich model			Dubinin-Radushkevich model			
Temperature (K)	Q_m (mg/g)	K_L (L/mg)	R^2	$1/n$	K_F $(mg/g)^{1/n}$	R^2	β (mol^2/J^2)	Q_m (mg/g)	E (kJ/mol)	R^2
298	769.23	0.001	0. 879	0.904	1.875	0.998	0.0003	174.75	40.82	0.874
303	679.52	0.002	0.723	0.909	1.850	0.997	0.0002	174.33	50	0.843
313	555.56	0.003	0.879	0.825	2.745	0.996	0.0002	166.75	50	0.843

Table 3
Thermodynamic parameters for OFL adsorption on BC

T (K)	K (L/mol)	ΔG (kJ/mol)	ΔS (J/mol K)	ΔH (kJ/mol)
298	99316	−64.87		
303	84194	−64.60	−83	−86
313	60226	−64.53		

the temperature from 298 K to 313 K, indicating that the adsorption process was an exothermic process [48]. Hence, the cotton stalk BC exhibited a high adsorption capacity.

3.5. Adsorption thermodynamics

The thermodynamic parameters for the adsorption of OFL are summarized in Table 3. The negative values of ΔG in the temperature range of 298–313 K indicate that the adsorption process of OFL has a degree of spontaneity and that adsorption is favorable. Moreover, the negative values of ΔH indicate that the adsorption was exothermic, which is consistent with the observations for the effect of temperature and the Langmuir isotherm model during the adsorption process. Finally, the negative values of ΔS indicate that randomness decreased during OFL adsorption [49].

4. Conclusion

This work demonstrates that BC prepared from cotton stalk shows good potential as an OFL adsorbent. SEM analysis revealed that the BC had a coarse surface and well-developed porous structure. The BC had a high surface area of 1196.224 m^2/g. The OFL adsorption experimental data were best fitted with a pseudo-second-order kinetic model ($R^2 > 0.998$) and the Freundlich isotherm model ($R^2 > 0.996$). Additionally, the thermodynamic parameters suggested that the OFL adsorption was spontaneous. Finally, abundant phosphorus-containing groups and C–O–C, C=O, C=C, P=O, P–O–C, and O–C moieties were detected on the BC surface.

Acknowledgements

This work was supported by the National Natural Science Foundation of China (No. 51708340), Major Science and Technology Program for Water Pollution Control and Treatment (2017ZX07101-001), International Postdoctoral Exchange Fellowship Program (No. 20180063), Promotional Research Fund for Excellent Young and Middle-aged Scientists of Shandong Province (ZR2016CB18) and Project of Shandong Province Higher Educational Science and Technology Program (No. J18KA186).

References

[1] J.P. Monk, D.M. Campoli-Richards, Ofloxacin, Drugs, 33 (1987) 346–391.
[2] P.A. Todd, D. Faulds, Ofloxacin. A reappraisal of its antimicrobial activity, pharmacology and therapeutic use, Drugs, 42 (1991) 825.
[3] W. Ben, Z. Qiang, X. Pan, M. Chen, Removal of veterinary antibiotics from sequencing batch reactor (SBR) pretreated swine wastewater by Fenton's reagent, Water Res., 43 (2009) 4392–4402.
[4] M. Schallenberg, A. Armstrong, Assessment of antibiotic activity in surface water of the lower Taieri Plain and impacts on aquatic bacteria in Lake Waipori, South Otago, New Zealand, New Zealand J. Mar. Fresh. Res., 38 (2004) 19–28.
[5] C.B. Özkal, Occurence of antibiotics in urban wastewater: A risk assessment study in Tekirdağ city related to antibiotic resistant bacteria and infection disease control, Chem. Commun., 46 (2014) 421–423.
[6] V. Bhatia, A.K. Ray, A. Dhir, Enhanced photocatalytic degradation of ofloxacin by co-doped titanium dioxide under solar irradiation, Sep. Purif. Technol., 161 (2016) 1–7.
[7] M. Crespo-Alonso, V.M. Nurchi, R. Biesuz, G. Alberti, N. Spano, M.I. Pilo, G. Sanna, Biomass against emerging pollution in wastewater: Ability of cork for the removal of ofloxacin from aqueous solutions at different pH, J. Environ. Chem. Eng., 1 (2013) 1199–1204.
[8] S.K. Mehta, P. Kundu, A. Kaur, S.K. Kansal, Removal of ofloxacin from aqueous phase using Ni-doped TiO_2 nanoparticles under solar irradiation, J. Nanosci. Nanotechnol., 14 (2014) 6991–6995.
[9] J.B. Carbajo, A.L. Petre, R. Rosal, S. Herrera, P. Letón, E. García-Calvo, A.R. Fernández-Alba, J.A. Perdigón-Melón, Continuous ozonation treatment of ofloxacin: Transformation products, water matrix effect and aquatic toxicity, J. Hazard. Mater., 292 (2015) 34–43.
[10] B.H. Hameed, A.A. Ahmad, Batch adsorption of methylene blue from aqueous solution by garlic peel, an agricultural waste biomass, J. Hazard. Mater., 164 (2009) 870.
[11] Q. Kong, X. He, L. Shu, M.S. Miao, Ofloxacin adsorption by activated carbon derived from luffa sponge: Kinetic, isotherm, and thermodynamic analyses, Process. Saf. Environ., (2017).
[12] D. Hui, J. Lu, G. Li, G. Zhang, X. Wang, Adsorption of methylene blue on adsorbent materials produced from cotton stalk, Chem. Eng. J., 172 (2011) 326–334.
[13] X.U. Yong-Jian, G. Pan, W.U. Yang-Yu, L.L. Fan, Effects of dynamic extruding on the properties of high yield cotton stalk pulp, Paper Paper Mak., (2011).

[14] A.M. Nour, A.E. Tag-El-Din, A.A. Nour, N.H. Ismail, M.A. Abaza, The use of cotton stalks in ruminants feeding. 2.- effect of using feed block licks and polymers on the nutritive value of cotton stalks and growth performance of Rahmany lambs, Alexandria J. Agri. Res., (1996).
[15] Singh, Surjit, Nahil, A. Mohamad, Wu, Chunfei, Williams, T. Paul, Xi, Novel application of cotton stalk as a waste derived catalyst in the low;temperature SCR-deNO(x) process, Fuel, 105 (2013) 585–594.
[16] Z.M. El, E. Smith, Modeling of heavy metals removal from aqueous solution using activated carbon produced from cotton stalk, Water Sci. Technol., 67 (2013) 1612–1619.
[17] A.M.A. Nada, N.A. El-Wakil, M.L. Hassan, A.M. Adel, Differential adsorption of heavy metal ions by cotton stalk cation-exchangers containing multiple functional groups, J. Appl. Polym. Sci., 101 (2006) 4124–4132.
[18] K. Li, Z. Zheng, J. Feng, J. Zhang, X. Luo, G. Zhao, X. Huang, Adsorption of p-nitroaniline from aqueous solutions onto activated carbon fiber prepared from cotton stalk, J. Hazard. Mater., 166 (2009) 1180–1185.
[19] M.J. Ahmed, S.K. Theydan, Fluoroquinolones antibiotics adsorption onto microporous activated carbon from lignocellulosic biomass by microwave pyrolysis, J. Taiwan Inst. Chem. E., 45 (2014) 219–226.
[20] H.Y. Zhang, Z.W. Wang, J.H. Gao, J.M. Zhu, C.R. Xie, X.Y. Xie, Adsorption characteristics of norfloxacin by biochars derived from reed straw and municipal sludge, Huan Jing Ke Xue, 37 (2016) 689–696.
[21] D.J. O'Shannessy, D.J. Winzor, Interpretation of deviations from pseudo-first-order kinetic behavior in the characterization of ligand binding by biosensor technology, Anal. Biochem., 236 (1996) 275.
[22] Y.S. Ho, A.E. Ofomaja, Pseudo-second-order model for lead ion sorption from aqueous solutions onto palm kernel fiber, J. Hazard. Mater., 129 (2006) 137–142.
[23] M. Goto, T. Hirose, Approximate rate equation for intraparticle diffusion with or without reaction, Chem. Eng. Sci., 48 (1993) 1912–1915.
[24] H.G. Carter, K.G. Kibler, Langmuir-type model for anomalous moisture diffusion in composite resins, J. Compos. Mater., 12 (1978) 118–131.
[25] G.P. Jeppu, T.P. Clement, A modified Langmuir-Freundlich isotherm model for simulating pH-dependent adsorption effects, J. Contam. Hydrol., 129–130 (2012) 46.
[26] C. Nguyen, D.D. Do, The Dubinin–Radushkevich equation and the underlying microscopic adsorption description, Carbon, 39 (2001) 1327–1336.
[27] A.L. Myers, J.M. Prausnitz, Thermodynamics of mixed-gas adsorption, AIChE J., 11 (1965) 121–127.
[28] W. Li, Z. Jian, Z. Ran, C. Zhang, L. Cong, L. Ye, Adsorption of 2,4-dichlorophenol on Mn-modified activated carbon prepared from Polygonum orientale Linn, Desalination, 266 (2011) 175–181.
[29] Q. Kong, Q. Liu, M.S. Miao, Y.Z. Liu, Q.F. Chen, C.S. Zhao, Kinetic and equilibrium studies of the biosorption of sunset yellow dye by alligator weed activated carbon, Desal. Water. Treat., 66 (2017) 281–290.
[30] J. Fan, J. Zhang, C. Zhang, L. Ren, Q. Shi, Adsorption of 2,4,6-trichlorophenol from aqueous solution onto activated carbon derived from loosestrife, Desalination, 267 (2011) 139–146.
[31] Z. Qi, Q. Liu, Z.R. Zhu, Q. Kong, Q.F. Chen, C.S. Zhao, Y.Z. Liu, M.S. Miao, C. Wang, Rhodamine B removal from aqueous solutions using loofah sponge and activated carbon prepared from loofah sponge, Desal. Water. Treat., 57(60) (2016) 29421–29433.
[32] N. Yalçın, V. Sevinç, Studies of the surface area and porosity of activated carbons prepared from rice husks, Carbon, 38 (2000) 1943–1945.
[33] S. Kizito, S. Wu, W.K. Kirui, L. Ming, Q. Lu, H. Bah, R. Dong, Evaluation of slow pyrolyzed wood and rice husks biochar for adsorption of ammonium nitrogen from piggery manure anaerobic digestate slurry, Sci. Total Environ., 505 (2015) 102–112.
[34] C.H. Chia, B. Gong, S.D. Joseph, C.E. Marjo, P. Munroe, A.M. Rich, Imaging of mineral-enriched biochar by FTIR, Raman and SEM–EDX, Vib. Spectrosc., 62 (2012) 248–257.
[35] A.M. Puziy, O.I. Poddubnaya, A. Martı Nez-Alonso, F. Suárez-Garcı A, J.M.D. Tascón, Synthetic carbons activated with phosphoric acid : I. Surface chemistry and ion binding properties, Carbon, 40 (2002) 1493–1505.
[36] N. Zhu, T. Yan, J. Qiao, H. Cao, Adsorption of arsenic, phosphorus and chromium by bismuth impregnated biochar: Adsorption mechanism and depleted adsorbent utilization, Chemosphere, 164 (2016) 32–40.
[37] W. Wu, M. Yang, Q. Feng, K. Mcgrouther, H. Wang, H. Lu, Y. Chen, Chemical characterization of rice straw-derived biochar for soil amendment, Biomass Bioenerg., 47 (2012) 268–276.
[38] M. Miao, Y. Wang, Q. Kong, L. Shu, Adsorption kinetics and optimum conditions for Cr(VI) removal by activated carbon prepared from luffa sponge, Desal. Water. Treat., 57 (2016) 7763–7772.
[39] G. Crini, P.-M. Badot, Application of chitosan, a natural aminopolysaccharide, for dye removal from aqueous solutions by adsorption processes using batch studies: A review of recent literature, Prog. Polym. Sci., 33 (2008) 399–447.
[40] C.L. Amorim, A.S. Maia, R.B. Mesquita, A.O. Rangel, M.C. van Loosdrecht, M.E. Tiritan, P.M. Castro, Performance of aerobic granular sludge in a sequencing batch bioreactor exposed to ofloxacin, norfloxacin and ciprofloxacin, Water Res., 50 (2014) 101–113.
[41] D.G. Larsson, C. de Pedro, N. Paxeus, Effluent from drug manufactures contains extremely high levels of pharmaceuticals, J. Hazard. Mater., 148 (2007) 751–755.
[42] S. Abbaszadeh, S.R.W. Alwi, C. Webb, N. Ghasemi, I.I. Muhamad, Treatment of lead-contaminated water using activated carbon adsorbent from locally available papaya peel biowaste, J. Clean. Prod., 118 (2016) 210–222.
[43] A. Saeed, M. Sharif, M. Iqbal, Application potential of grapefruit peel as dye sorbent: kinetics, equilibrium and mechanism of crystal violet adsorption, J. Hazard. Mater., 179 (2010) 564–572.
[44] F. Kaouah, S. Boumaza, T. Berrama, M. Trari, Z. Bendjama, Preparation and characterization of activated carbon from wild olive cores (oleaster) by H_3PO_4 for the removal of Basic Red 46, J. Clean. Prod., 54 (2013) 296–306.
[45] H. Laksaci, A. Khelifi, M. Trari, A. Addoun, Synthesis and characterization of microporous activated carbon from coffee grounds using potassium hydroxides, J. Clean. Prod., 147 (2017) 254–262.
[46] S. Azizian, Kinetic models of sorption: a theoretical analysis, J. Colloid Interface Sci., 276 (2004) 47.
[47] M.T. Amin, A.A. Alazba, M. Shafiq, Adsorptive removal of Reactive Black 5 from wastewater using bentonite clay: isotherms, kinetics and thermodynamics, Sustainability, 7 (2015) 15302–15318.
[48] Y. Tian, P. Liu, X. Wang, H. Lin, Adsorption of malachite green from aqueous solutions onto ordered mesoporous carbons, Chem. Eng. J., 171 (2011) 1263–1269.
[49] V.K. Gupta, A. Mittal, L. Krishnan, V. Gajbe, Adsorption kinetics and column operations for the removal and recovery of malachite green from wastewater using bottom ash, Sep. Purif. Technol., 40 (2004) 87–96.